

Coversheet for EarthArXiv

Title:

A late response of the sea-ice cover to Neoglacial cooling in the western Barents Sea

Authors:

M M Telesiński – Institute of Oceanology Polish Academy of Sciences, Powstańców
Warszawy 55, Sopot 81-712, Poland

M Kucharska – Institute of Oceanology Polish Academy of Sciences, Powstańców
Warszawy 55, Sopot 81-712, Poland

M Łącka – Institute of Oceanology Polish Academy of Sciences, Powstańców
Warszawy 55, Sopot 81-712, Poland

M Zajączkowski – Institute of Oceanology Polish Academy of Sciences, Powstańców
Warszawy 55, Sopot 81-712, Poland

Author Email Addresses:

M M Telesiński (mtelesinski@iopan.pl)

M Kucharska (kucharska.m89@gmail.com)

M Łącka (mlacka@iopan.pl)

M Zajączkowski (trapper@iopan.pl)

Peer Review Statement:

This is a non-peer-reviewed preprint submitted to EarthArXiv. The work has been submitted to the journal The Holocene for review.

1 **Title: A late response of the sea-ice cover to Neoglacial cooling in the western**
2 **Barents Sea**

3 **Author names and affiliations**

4 Maciej M. Telesiński^a, Małgorzata Kucharska^a, Magdalena Łacka^a, Marek
5 Zajączkowski^a

6 ^aInstitute of Oceanology Polish Academy of Sciences, Powstańców Warszawy 55,
7 Sopot 81-712, Poland

8 **Abstract**

9 In high northern latitudes, the Middle to Late Holocene was a time of orbitally-induced
10 atmospheric cooling. This led to increased sea-ice production in the Arctic Ocean and its export
11 southward, a decrease in sea surface temperatures (SST), and glacier advances at least since 5-
12 4 ka BP. However, the response of the ocean-climate system to decreasing insolation was not
13 uniform. Our research shows that the sea-ice cover in the northwestern Barents Sea experienced
14 a late response to Neoglacial cooling. We analysed dinoflagellate cyst assemblages from a
15 sediment core from Storfjordrenna, south of Svalbard, and found that the area experienced ice-
16 free conditions throughout most of the Mid- and Late Holocene. It was only after 2.3 ka BP that
17 the study site became covered with winter drift ice and primary productivity decreased
18 subsequently. Other data from the region support the decrease in SST, the expansion of the sea-
19 ice cover, and the deterioration of the environmental conditions around that time. Our findings
20 indicate that the sea-ice cover in the northwestern Barents Sea required a significant amount of
21 time to respond to the general cooling trend in the region. These results have important
22 implications for present-day environmental changes. Even if the current warming trend is
23 revoked in the future, the observed sea-ice loss in the Barents Sea may be incredibly challenging
24 to reverse.

25 **Introduction**

26 The Middle to Late Holocene in high northern latitudes was a time of decreasing
27 temperatures (McKay et al., 2018) caused by declining boreal summer insolation (Laskar et al.,
28 2004) and referred to as Neoglacial cooling (Wanner, 2021). Around 5 ka BP the modern sea
29 level was reached and the postglacial flooding of the Laptev Sea shelves was finalized (Bauch
30 et al., 2001), allowing the Arctic sea-ice production, which predominantly takes place on the
31 shallow Arctic shelf areas, to reach its modern magnitude (Werner et al., 2013). This resulted

32 in the onset of modern-like conditions with perennial sea ice in the Arctic Ocean (Cronin et al.,
33 2010). Enhanced mid-Holocene Siberian river runoff caused an eastward shift of Transpolar
34 Drift and increased sea-ice export through the Fram Strait (Dyke et al., 1997; Prange and
35 Lohmann, 2003). Data from the Greenland Ice Core Project ice core show the onset of
36 atmospheric cooling between 5 and 4 ka BP (Dahl-Jensen et al., 1998). Although in the northern
37 North Atlantic region there is no compelling evidence for any significant and widespread
38 climatic anomaly (Bradley and Bakke, 2019) associated with the 4.2 ka BP event (Renssen,
39 2022) that marks the onset of the Late Holocene (Walker et al., 2019), a compilation of glacier
40 records indicates a significant climatic transition referred to as 'the Holocene Turnover'
41 occurred ~4 ka BP. It represents a dynamical adjustment that subsequently resulted in the
42 establishment of a new climate regime or mode rather than being a multidecadal or centennial
43 deviation from mean conditions (Paasche et al., 2004; Paasche and Bakke, 2009). On Svalbard,
44 Late Holocene glacier re-advances started around 4 ka BP (Farnsworth et al., 2020). Tidewater
45 glaciers, which were largely absent in Svalbard during the early and mid-Holocene, reappeared
46 3-4 ka BP (Jang et al., 2023; Svendsen and Mangerud, 1997). Similarly, in northern Norway,
47 glaciers reappeared ~4 ka BP (Bakke et al., 2005). This coincides with the onset of sea surface
48 temperature (SST) decrease in the northwestern Barents Sea continental slope (Rigual-
49 Hernández et al., 2017; Risebrobakken et al., 2010). In the subpolar North Atlantic, pronounced
50 SST cooling was observed between 4 and 2 ka BP (Orme et al., 2018). A significant sea-ice
51 advance accompanied by distinct sea-ice fluctuations occurred in the eastern Fram Strait after
52 3 ka BP (Müller et al., 2012). By 2 ka BP, the SST in the Norwegian Sea had already decreased
53 to its Holocene low (Andersen, Koç, Jennings, et al., 2004). However, the response of the ocean
54 environment to decreasing boreal summer insolation was not uniform (Andersen, Koç and
55 Moros, 2004; Andersen, Koç, Jennings, et al., 2004; Wanner, 2021). Around 2 ka BP, the North
56 Atlantic Oscillation, the dominant mode of atmospheric variability at mid-latitudes in the North
57 Atlantic region, changed from variable, intermittently negative to generally positive conditions
58 (Olsen et al., 2012), indicating stronger westerlies. This caused increased Atlantic Water (AW)
59 advection into the Nordic Seas (e.g., Giraudeau et al., 2010; Spielhagen et al., 2011; Telesiński
60 et al., 2014, 2015; Werner et al., 2013). As a result, ocean (e.g., Andersen, Koç, Jennings, et
61 al., 2004; Sarnthein et al., 2003) as well as atmospheric (e.g., Johnsen et al., 2001; McDermott
62 et al., 2001) warming occurred. In Europe and the North Atlantic region, it is recognized as the
63 Roman Warm Period (e.g., Bianchi and McCave, 1999; Matul et al., 2018; Wang et al., 2012).

64 Here we reconstruct paleoenvironmental changes in the northwestern Barents Sea
65 during the Late Holocene to estimate how fast the sea-ice cover reacted to changes in the
66 atmosphere and the ocean. We analyse proxy data from a marine sediment core from
67 Storfjordrenna, south of Svalbard, including dinoflagellate cyst (dinocyst) assemblages, as well
68 as previously published XRF data, stable isotope and alkenone-based SST records. Based on
69 the abundance of indicator species of dinocysts, we reconstruct the reappearance of winter drift
70 ice, as well as the changing influence of AW on the study site. We also compare our data with
71 biomarker-based reconstruction of sea ice from a core from the Olga Basin, northern Barents
72 Sea (Berben et al., 2017).

73 **Oceanographic setting**

74 The Barents Sea is an Arctic shelf sea between the Nansen Basin of the Arctic Ocean to
75 the north, Novaya Zemlya to the east, Scandinavia to the south, the Norwegian Sea to the west,
76 and the Svalbard archipelago to the north-west (Fig. 1). The Barents Sea is influenced by several
77 water masses. For this reason, strong environmental gradients can be observed here, making it
78 a great area for studying paleoceanographic changes (e.g., Berben et al., 2017; Knies et al.,
79 2017; Łacka et al., 2015, 2019).

80 The relatively warm and saline AW ($T > 3^{\circ}\text{C}$, $S > 35.0$; Loeng, 1991) is carried northward
81 by the Norwegian Atlantic Current (Hopkins, 1991). The current is divided into the West
82 Spitsbergen Current (WSC) and the North Cape Current. The North Cape Current enters the
83 Barents Sea directly from the south-west, through Bjørnøyrenna, while the WSC continues
84 northward along the shelf break, encircles Svalbard (Manley, 1995) and enters the Barents Sea
85 from the north as a subsurface current, through Franz Victoria Trough (Abrahamsen et al., 2006;
86 Rudels et al., 2015). Subsequently, AW is advected southwestward into the Olga Basin, where
87 it has been observed year-round (Abrahamsen et al., 2006). After mixing and heat loss, AW
88 exits the Barents Sea and reaches the Arctic Ocean via the St. Anna Trough (e.g., Rudels et al.,
89 2015; Schauer et al., 2002).

90 The Polar Water (PW) is brought from the Arctic Ocean into the Barents Sea through
91 the Franz Victoria and St. Anna Troughs, via the East Spitsbergen Current and the Bear Island
92 Current, respectively. Arctic Water (ArW) is formed when relatively warm AW mixes with
93 cold, less saline, and ice-loaded PW (Hopkins, 1991). Hence, surface water in the north-eastern
94 Barents Sea is dominated by ArW, characterised by reduced temperature and salinity, as well
95 as seasonal sea ice conditions (Hopkins, 1991).

96 The main oceanographic features of the near-surface waters of the Barents Sea are the
97 oceanic fronts (Pfirman et al., 1994). Defined as sharp gradients in terms of temperature, salinity
98 and sea ice, the Polar and Arctic fronts are the respective boundaries between PW/ArW and
99 ArW/AW. The positions of the Polar and Arctic fronts are closely related to the overall sea ice
100 conditions and, in particular, align with the average summer and winter sea ice margins,
101 respectively (Vinje, 1977). Although sea ice advection from the Arctic Ocean occurs, sea ice
102 within the Barents Sea is formed mainly locally during autumn and winter (Loeng, 1991). The
103 southward extent of the oceanic fronts and the sea-ice conditions are regulated by the inflow of
104 AW into the western Barents Sea (Årthun et al., 2012), though in the west the PF is
105 topographically controlled and therefore rather stable (Lien et al., 2017). On the contrary, the
106 north-eastern Barents Sea experiences large changes in seasonal sea-ice conditions (Sorteberg
107 and Kvingedal, 2006; Vinje, 2001) with maximum sea-ice conditions during March/April and
108 minimum occurring throughout August/September.

109 The interplay between water masses determines the position of the marginal ice zone
110 (MIZ) (Divine and Dick, 2006), an area characterised by high surface productivity during the
111 summer season (e.g. Smith and Sakshaug, 1990). Within the Barents Sea, enhanced primary
112 production results from a peak algal bloom along the MIZ as sea ice retreats in late spring
113 (Hebbeln and Wefer, 1991; Ramseier et al., 1999; Sakshaug, 2004). Additionally, AW
114 advection contributes to longer productive seasons, compared to other Arctic areas (Wassmann,
115 2011). Consequently, the Barents Sea is one of the most productive areas of the Arctic seas
116 (Wassmann, 2011; Wassmann et al., 2006).

117 **Material and methods**

118 Sediment gravity core JM09-020 was retrieved from Storfjordrenna, northwestern
119 Barents Sea (Fig. 1, 76°19' N, 19°42' E, 253 m water depth, Łacka et al., 2015) and has been
120 successfully used to reconstruct paleoceanographic conditions in the area over the last 14 kyr
121 (Łacka et al., 2015, 2019, 2020).

122 For dinocyst analysis, the core was sampled every 4-6 cm. Each 1-cm-thick slab of
123 sediment was collected into a zip bag and stored at a temperature of -20°C. After thawing, 3-4
124 cm³ of well-mixed sediment was put in a polypropylene test tube, dried at >40°C and weighed
125 with an analytical balance. Samples were subsequently soaked with distilled water for 12 h,
126 centrifuged at 3600 rpm for 6 min and then processed using a standard palynological technique
127 (e.g., Pospelova et al., 2005, 2010).

128 Marker grains of a known number of *Lycopodium clavatum* spores (e.g., Mertens et al.,
129 2009; Mertens, Price, et al., 2012) were added to allow quantitative estimates of the absolute
130 concentrations of dinocysts. At room temperature, about 7 ml of hydrochloric acid (HCl, 10%)
131 was slowly added to samples to dissolve the *L. clavatum* spore tablets and remove carbonates.
132 After 30 minutes samples were centrifuged and decanted. Subsequently, ~9 ml of distilled water
133 was added and samples were centrifuged and decanted again. The procedure was repeated until
134 the pH of the supernatant reached a neutral level. Afterwards, the samples were wet-sieved
135 through 125 μm and 15 μm mesh to remove fractions of sediment above and below the maximal
136 and minimal size of dinocysts.

137 After sieving, centrifuging, and decanting, ~7 ml of room-temperature hydrofluoric acid
138 (HF, 48%) was added to the sediment to remove silicate. Samples were left in a fume hood for
139 72 hours, with regular digestion checking and stirring. After silicate dissolution, samples were
140 once again centrifuged and decanted and ~7 ml of hydrochloric acid (HCl, 10%, at room
141 temperature) was added. Samples were rinsed with distilled water as described above and sieved
142 through a 15 μm mesh. Aliquots of a few drops of sample residue were placed on a glass slide
143 and left for 24 h at room temperature to dry. Glycerine gel was used to mount a cover slide to
144 the glass slide.

145 Approximately 300 dinocyst specimens (min 201, max 341) were counted from each
146 sample. Dinocysts were identified to the lowest possible taxonomical level. The paleontological
147 taxonomy system used throughout this paper follows Zonneveld (1997), Kunz-Pirrung (1998),
148 Montresor et al. (1999), Rochon et al. (1999), Head et al. (2001), Pospelova and Head (2002),
149 Moestrup et al. (2009), Mertens et al. (2013, 2015; 2012), and Zonneveld and Pospelova (2015).
150 Cysts with unknown taxonomic affinity were classified into one of four groups: unidentified 1
151 – round transparent cyst, unidentified 2 – spiny transparent cyst, RBC – round brown cyst and
152 SBC – spiny brown cyst. Cysts of *Biecheleria cf. baltica* are mostly very small (~5–10 μm) and
153 were partly lost during sample preparation (sieving). Therefore, we excluded them from the
154 total cyst concentrations statistical analyses. Furthermore, it cannot be excluded that some thin-
155 walled transparent *Impagidinium* spp. cysts have been missed during the counting (Telesiński
156 et al., 2023).

157 The chronology of core JM09-020 was based on radiocarbon dating (Łacka et al., 2015).
158 We recalibrated the AMS ^{14}C dates using CALIB ^{14}C age calibration software (rev 8.1.0;
159 Stuiver and Reimer, 1993) and the Marine20 calibration curve (Heaton et al., 2020). A regional
160 correction of $\Delta R = -53 \pm 36$ ^{14}C years was applied. This value was calculated with the Marine

161 Reservoir Correction database (Reimer and Reimer, 2001) and the Marine20 curve (Heaton et
162 al., 2020, 2022) using the same mollusc samples as those used by Mangerud et al. (2006) for
163 Svalbard. The difference between the resulting and the original age model (Łącka et al., 2015)
164 is less than 50 years within the Holocene, which is insignificant for the present study, allowing
165 for a direct comparison with previous studies of the core (Łącka et al., 2015, 2019).

166 **Results**

167 Here we present only selected parameters of the dinocyst assemblage analysis that are
168 important for the current study. Complete results can be found in the Supplementary Material.
169 Total dinocyst abundance was low (<5k cysts g⁻¹) in the earliest Holocene (Fig. 2A). It increased
170 rapidly to >20k cysts g⁻¹ around 11 ka BP. Subsequently, the abundance decreased gradually to
171 ~7.5k cysts g⁻¹ around 7.5 ka BP and then increased to reach a maximum of 35k cysts g⁻¹ at 2.5
172 ka BP. In the youngest part of the record, the abundance decreased again to reach ~15k cysts g⁻¹
173 at 1.3 ka BP. The dinocyst assemblage was generally dominated by heterotrophic species (Fig.
174 2B). However, the percentage of autotrophic dinocysts was gradually increasing from <5% in
175 the Early Holocene to a maximum of 51% at 2.3 ka BP. Subsequently, the percentage of
176 autotrophic cysts decreased again to 21% at the end of the record. The abundance of
177 *Echinidinium karaense* was relatively high in the Early Holocene, though it never exceeded a
178 relative abundance of 5% or an absolute abundance of 300 cysts g⁻¹ (Fig. 2C). After 8 ka BP
179 the species disappeared completely from the record and reappeared only around 2.1 ka BP,
180 though in lower relative and absolute abundances than in the Early Holocene (up to 1.3% and
181 200 cysts g⁻¹, respectively). The abundance of *Operculodinium centrocarpum* s.l. was
182 extremely low throughout the Early Holocene (Fig. 2D). Starting from 7.5 ka BP, it increased
183 gradually to reach a maximum of 44% (10.9k cysts g⁻¹) around 2.3 ka BP and subsequently
184 decreased to 17% (2.6k cysts g⁻¹) towards the end of the record. The relative abundance of
185 *Islandinium minutum* (Fig. 2E) in the earliest Holocene was high (10-20%), though its absolute
186 abundance remained relatively low (<1k cysts g⁻¹). Between 11 ka BP and 2.1 ka BP both
187 relative and absolute abundance was low. Only around 2.1 ka BP both relative and absolute
188 abundance of this species increased to approximately 20% and 3k cysts g⁻¹, respectively, and
189 remained high until the end of the record.

190 **Discussion**

191 The dinocyst species *Echnidinium karaense*, together with cysts of *Polarella glacialis*,
192 has recently been identified as a winter drift ice indicator in waters around Svalbard (Telesiński
193 et al., 2023). As the latter species is virtually absent in core JM09-020 (Supplementary

194 Material), *Echinidinium karaense* remains the only available dinocyst sea-ice indicator. It was
195 present in the western Barents Sea over the Early Holocene but it disappeared around 8 ka BP
196 (Fig. 2C), indicating ice-free conditions. Its reappearance in around 2.1 ka BP, after almost 6
197 thousand years of absence, clearly indicates a return of sea-ice conditions comparable to those
198 in the Early Holocene. This is further supported by other dinocyst data from the same core. The
199 peak in total dinocyst abundance at 2.5 ka BP (Fig. 2A), followed by a peak in autotrophic
200 dinocyst abundance shortly thereafter (Fig. 2B), indicates increased primary productivity,
201 which might suggest that the core site was reached by the MIZ (e.g., Barber et al., 2015;
202 Ramseier et al., 1999; Sakshaug, 2004). After ~2 ka BP the total and autotrophic dinocyst
203 abundance decreased, suggesting deteriorating surface water conditions, possibly due to the
204 thickening of the sea-ice cover. Similarly, the abundance of *Operculoidinium centrocarpum*
205 s.l., a cosmopolitan species whose high abundances in high northern latitudes are associated
206 with AW dominance (Grøsfjeld et al., 2009; Rochon et al., 1999; Telesiński et al., 2023)
207 reached a maximum around 2.3 ka BP but decreased sharply shortly thereafter, though remained
208 higher than in the first half of the Holocene (Fig. 2D). Furthermore, the relative percentage of
209 *O. centrocarpum* s.l. versus *I. minutum*, which was relatively high throughout most of the Late
210 Holocene (Fig. 3C), decreased after 2.1 ka BP. The relative percentage of these two species
211 may be used to indicate whether warm AW flows at the surface or as a subsurface water mass
212 (Grøsfjeld et al., 2009). This suggests that until 2.1 ka BP, AW remained at the surface in the
213 northwestern Barents Sea, while it subducted below ArW thereafter.

214 Additional evidence from core JM09-020 corroborates the dinocyst data. An SST
215 reconstruction based on alkenones (Łącka et al., 2019) shows a clear cooling trend between 2.3
216 and 2 ka BP (Fig. 3D), which could be attributed to the expansion of sea ice. Similarly, the
217 stable carbon isotope values of benthic foraminifera (Łącka et al., 2015) indicate increased
218 variability in environmental conditions after 2 ka BP on the sea bottom (Fig. 3E), which could
219 be linked to enhanced sea-ice cover, variable productivity at the sea surface, and the amount of
220 organic matter reaching the sea floor. Further details are provided by XRF data (Łącka et al.,
221 2015). The Ba/Ti ratio exhibits a stepwise decrease around 2.3 ka BP (Fig. 3F). Since the Ba/Ti
222 ratio is believed to be broadly proportional to the organic carbon content in sediment (Thomson
223 et al., 2006), such a decrease could indicate declining productivity (Croudace et al., 2006).

224 Based on the available data, it is evident that the northwestern Barents Sea witnessed a
225 period of maximum productivity around 2.5-2.3 ka BP. This was mainly due to the inflow of
226 warm surface AW from the west and the migration of the MIZ from the east. However, after

227 2.3-2.1 ka BP, the study site was covered with sea-ice and the AW submerged below surface
228 ArW, which resulted in a decrease in SST and productivity.

229 Our results are further confirmed by data from core NP05-11-70GC from the Olga
230 Basin, east of Svalbard (Berben et al., 2017). The $P_{III}IP_{25}$ index combines concentrations of tri-
231 unsaturated highly branched isoprenoid (HBI) lipid (HBI III), a phytoplankton-derived
232 biomarker, with IP_{25} , a sea-ice proxy, to investigate past sea-ice conditions more quantitatively
233 (Belt et al., 2007; Berben et al., 2017; Müller et al., 2011). The Olga Basin record indicates a
234 constant increase in sea-ice concentration over the Holocene (Berben et al., 2017). Around 2.8
235 ka BP, the $P_{III}IP_{25}$ index crossed the 0.8 threshold (Fig. 3G), indicating >5% summer sea-ice
236 concentration (Smik et al., 2016). Around 2.5 ka BP, spring sea-ice concentration in the Olga
237 Basin, derived from the $P_{III}IP_{25}$ index (Berben et al., 2017), reached 70%. Finally, around 1.9
238 ka BP, another stepwise increase of the $P_{III}IP_{25}$ index (approximately equal to eight of the total
239 Holocene increase) occurred. The data from the Olga Basin confirm that a strong environmental
240 gradient characterised the Barents Sea also in the past. While in the northern part of the basin,
241 a dense spring sea-ice concentration was reached already around 2.5 ka BP, in the western part
242 winter drift ice only appeared around 2.1 ka BP (Fig. 3B and G). Nevertheless, data from both
243 records confirm that the sea-ice cover reacted slowly to the Neoglacial cooling. Similarly,
244 oxygen isotope data from core NP05-71GC from south of Kvitøya (Klitgaard-Kristensen et al.,
245 2013) suggest that after *c.* 2.5 ka BP the northwestern Barents Sea experienced cooling and/or
246 increased brine formation, most probably related to the sea-ice expansion.

247 All the presented data suggest that the sea-ice expansion in the north-western Barents
248 Sea occurred around 2.5-2.1 ka BP. Such a late response of the sea-ice cover to Neoglacial
249 cooling is surprising. Firstly, the Arctic sea-ice production on the Siberian shelves has reached
250 its modern magnitude already around 5 ka BP (Bauch et al., 2001; Werner et al., 2013) causing
251 perennial sea-ice cover in the Arctic Ocean (Cronin et al., 2010). The fact that the sea-ice cover
252 in the Barents Sea did not respond to this increase can be explained by the minor influence of
253 advected (as opposed to locally formed) sea ice on the basin's ice budget during the Late
254 Holocene (Loeng, 1991). On the other hand, terrestrial data indicate that the glacier re-advance
255 in Svalbard began as early as ~4 ka BP (Farnsworth et al., 2020; Jang et al., 2023; Svendsen
256 and Mangerud, 1997), suggesting that the atmospheric cooling in the north-western Barents Sea
257 region required for the glacier growth was already achieved at the beginning of the Late
258 Holocene.

259 The approximately 2 kyr delay of the sea-ice expansion relative to the onset of
260 atmospheric cooling and glacier advance in the region indicates that sea-ice cover in the Barents
261 Sea needed significant time to recover, even in favourable climatic conditions. This was
262 probably caused by the strong influence of AW, whose intrusions into the Barents Sea were
263 frequent during the Middle and Late Holocene (e.g., Pawłowska et al., 2020; Risebrobakken et
264 al., 2010). It is worth noting that in core JM09-020, the abundance of the AW-indicating species
265 *Operculoidinium centrocarpum* s.l. reached its maximum only ~2.3 ka BP (Fig. 3C) and SST
266 as well as productivity remained high until that time (Fig. 3D and F), suggesting that in the
267 western Barents Sea, the influence of AW was still increasing well into the Late Holocene,
268 despite the ongoing expansion of the sea-ice cover in the northern and eastern parts of the basin
269 (Berben et al., 2017).

270 In the western Barents Sea, the PF is currently mainly topographically controlled (Lien
271 et al., 2017). However, during the warm middle Holocene, the PF most probably decoupled
272 from the bottom topography, allowing AW to reach much farther to the northeast (e.g., Berben
273 et al., 2017). As a result, when orbitally forced Neoglacial cooling began, time was needed to
274 push surface AW out of the central part of the Barents Sea, whereas in the west AW could have
275 even increased its inflow on the surface. Even when atmospheric cooling in the region was
276 advanced enough ~4 ka BP to allow the advance of Svalbard glaciers, another ~2 kyr was
277 needed for the sea surface to cool enough to allow the sea ice to expand into the western Barents
278 Sea. On the other hand, open water in the vicinity of Svalbard must have been an important
279 source of moisture that allowed the growth of the glaciers (e.g., Hebbeln et al., 1994).

280 Over the last decades, AW intrusions on the Barents Sea shelf are becoming increasingly
281 common (Kujawa et al., 2021; Telesiński et al., 2023; Walczowski and Piechura, 2011) as a
282 result of enhanced northward heat transfer by the North Atlantic Drift (e.g., Spielhagen et al.,
283 2011; Walczowski and Piechura, 2007), a phenomenon referred to as ‘Atlantification’ of the
284 Barents Sea (e.g., Årthun et al., 2012; Tesi et al., 2021). The delayed response of the sea-ice
285 cover in the Barents Sea to Late Holocene cooling demonstrated in this study suggests that even
286 if the ongoing global warming is reversed in the future, which in itself is a highly challenging
287 task, many centuries might be required for the sea ice to recover to its preindustrial extent.
288 Taking into account that shrinking sea ice is one of the main drivers of the Arctic amplification
289 (Serreze and Francis, 2006) as it reduces surface albedo, leading to greater surface solar
290 absorption, amplifying warming and further melt (e.g., Curry et al., 1995; Thackeray and Hall,

291 2019), the currently observed rapid sea-ice loss (e.g., Overland and Wang, 2013) might be an
292 incredibly slow and long process to reverse.

293

294 **Summary and conclusions**

295 Reconstructing the paleoceanographic evolution of the northwestern Barents Sea during
296 the Late Holocene has been made possible by analyzing dinocyst assemblage data from
297 sediment core JM09-020 from Storfjordrenna, south of Svalbard. The dinocyst data has been
298 supplemented by stable carbon isotope, alkenone-based SST, and XRF data that have been
299 previously published (Łącka et al., 2015, 2019). Furthermore, the dinocyst data has been
300 compared with biomarker-based data from core NP05-11-70GC from the Olga Basin, east of
301 Svalbard (Berben et al., 2017).

302 Based on the data, it appears that despite the ongoing Neoglacial cooling that began
303 around 5 ka BP in high northern latitudes, between 2.5 and 2.3 ka BP, the northeastern Barents
304 Sea experienced a period of maximum productivity. This was due to two factors: the dominance
305 of warm AW on the surface, and the proximity of the MIZ. Only after 2.3-2.1 ka BP did winter
306 drift ice begin to cover the northwestern Barents Sea, resulting in a decrease in SST and
307 productivity due to the subduction of AW below ArW.

308 Our findings have important implications for the current and future environmental
309 changes. The presented data show that the recovery of the sea ice in the Barents Sea is a slow
310 process. Even if the ongoing global warming can be halted or even revoked in the future, the
311 reversing of the present sea-ice loss in the Barents Sea may be an incredibly long process.

312

313 **Acknowledgements**

314 This study was supported by grant no. 2020/39/B/ST10/01698 funded by the National
315 Science Centre, Poland. Supplementary Material, containing all the dinocyst data from core
316 JM09-020, is available on Zenodo (<https://doi.org/10.5281/zenodo.8322505>, Telesiński et al.
317 2023).

318

319 **References**

- 320 Abrahamsen EP, Østerhus S and Gammelsrød T (2006) Ice draft and current measurements
321 from the north-western Barents Sea, 1993–96. *Polar Research* 25(1): 25–37. DOI:
322 10.3402/polar.v25i1.6236.
- 323 Andersen C, Koç N and Moros M (2004) A highly unstable Holocene climate in the subpolar
324 North Atlantic : evidence from diatoms. *Quaternary Science Reviews* 23: 2155–2166.
325 DOI: 10.1016/j.quascirev.2004.08.004.
- 326 Andersen C, Koç N, Jennings AE, et al. (2004) Nonuniform response of the major surface
327 currents in the Nordic Seas to insolation forcing: Implications for the Holocene climate
328 variability. *Paleoceanography* 19: PA2003. DOI: 10.1029/2002PA000873.
- 329 Årthun M, Eldevik T, Smedsrud LH, et al. (2012) Quantifying the Influence of Atlantic Heat
330 on Barents Sea Ice Variability and Retreat. *Journal of Climate* 25(13): 4736–4743. DOI:
331 10.1175/JCLI-D-11-00466.1.
- 332 Bakke J, Dahl SO, Paasche Ø, et al. (2005) Glacier fluctuations, equilibrium-line altitudes and
333 palaeoclimate in Lyngen, northern Norway, during the Lateglacial and Holocene. *The*
334 *Holocene* 15(4): 518–540. DOI: 10.1191/0959683605hl815rp.
- 335 Barber DG, Hop H, Mundy CJ, et al. (2015) Selected physical, biological and biogeochemical
336 implications of a rapidly changing Arctic Marginal Ice Zone. *Progress in Oceanography*
337 139. Elsevier Ltd: 122–150. DOI: 10.1016/j.pocean.2015.09.003.
- 338 Bauch HA, Mueller-Lupp T, Taldenkova E, et al. (2001) Chronology of the Holocene
339 transgression at the North Siberian margin. *Global and Planetary Change* 31: 125–139.
340 DOI: 10.1016/S0921-8181(01)00116-3.
- 341 Belt ST, Massé G, Rowland SJ, et al. (2007) A novel chemical fossil of palaeo sea ice: IP25.
342 *Organic Geochemistry* 38: 16–27. DOI: 10.1016/j.orggeochem.2006.09.013.
- 343 Berben SMP, Husum K, Navarro-Rodriguez A, et al. (2017) Semi-quantitative reconstruction
344 of early to late Holocene spring and summer sea ice conditions in the northern Barents
345 Sea. *Journal of Quaternary Science* 32(5): 587–603. DOI: 10.1002/jqs.2953.
- 346 Bianchi GG and McCave IN (1999) Holocene periodicity in North Atlantic climate and deep-
347 ocean flow south of Iceland. *Nature* 397: 515–517. Available at:
348 <http://www.nature.com/nature/journal/v397/n6719/abs/397515a0.html> (accessed 15

349 January 2013).

350 Bradley RS and Bakke J (2019) Is there evidence for a 4.2 ka BP event in the northern North
351 Atlantic region? *Climate of the Past* (15): 1665–1676. DOI: 10.5194/cp-2018-162.

352 Cronin TM, Gemery L, Briggs WM, et al. (2010) Quaternary Sea-ice history in the Arctic
353 Ocean based on a new Ostracode sea-ice proxy. *Quaternary Science Reviews* 29(25–26).
354 Elsevier Ltd: 3415–3429. DOI: 10.1016/j.quascirev.2010.05.024.

355 Croudace IW, Rindby A and Rothwell RG (2006) ITRAX: Description and evaluation of a new
356 multi-function X-ray core scanner. *Geological Society Special Publication* 267(May
357 2016): 51–63. DOI: 10.1144/GSL.SP.2006.267.01.04.

358 Curry JA, Schramm JL and Ebert EE (1995) Sea Ice-Albedo Climate Feedback Mechanism.
359 *Journal of Climate* 8(2): 240–247. DOI: 10.1175/1520-
360 0442(1995)008<0240:SIACFM>2.0.CO;2.

361 Dahl-Jensen D, Mosegaard K, Gundestrup N, et al. (1998) Past temperatures directly from the
362 Greenland Ice Sheet. *Science* 282(5387): 268–271. DOI: 10.1126/science.282.5387.268.

363 Divine D V. and Dick C (2006) Historical variability of sea ice edge position in the Nordic
364 Seas. *Journal of Geophysical Research: Oceans* 111(1): 1–14. DOI:
365 10.1029/2004JC002851.

366 Dyke AS, England J, Reimnitz E, et al. (1997) Changes in driftwood delivery to the Canadian
367 Arctic Archipelago: The hypothesis of postglacial oscillations of the Transpolar Drift.
368 *Arctic* 50(1): 1–16. Available at:
369 <http://arctic.synergiesprairies.ca/arctic/index.php/arctic/article/view/1086> (accessed 5
370 March 2014).

371 Farnsworth WR, Allaart L, Ingólfsson Ó, et al. (2020) Holocene glacial history of Svalbard:
372 Status, perspectives and challenges. *Earth-Science Reviews* 208(October 2019). Elsevier:
373 103249. DOI: 10.1016/j.earscirev.2020.103249.

374 Giraudeau J, Grelaud M, Solignac S, et al. (2010) Millennial-scale variability in Atlantic water
375 advection to the Nordic Seas derived from Holocene coccolith concentration records.
376 *Quaternary Science Reviews* 29(9–10): 1276–1287. DOI:
377 10.1016/j.quascirev.2010.02.014.

378 Grøsfjeld K, Harland R and Howe J (2009) Dinoflagellate cyst assemblages inshore and

379 offshore Svalbard reflecting their modern hydrography and climate. *Norwegian Journal of*
380 *Geology* 89(1–2): 121–134.

381 Head MJ, Harland R and Matthiessen J (2001) Cold marine indicators of the late Quaternary:
382 The new dinoflagellate cyst genus *Islandinium* and related morphotypes. *Journal of*
383 *Quaternary Science* 16(7): 621–636. DOI: 10.1002/jqs.657.

384 Heaton TJ, Köhler P, Butzin M, et al. (2020) Marine20 — the Marine Radiocarbon Age
385 Calibration Curve (0 – 55,000 Cal Bp). *Radiocarbon* 00(00): 1–42. DOI:
386 10.1017/RDC.2020.68.

387 Heaton TJ, Bard E, Bronk Ramsey C, et al. (2022) A RESPONSE TO COMMUNITY
388 QUESTIONS ON THE MARINE20 RADIOCARBON AGE CALIBRATION CURVE:
389 MARINE RESERVOIR AGES AND THE CALIBRATION OF 14 C SAMPLES FROM
390 THE OCEANS. *Radiocarbon* 00(00): 1–27. DOI: 10.1017/RDC.2022.66.

391 Hebbeln D and Wefer G (1991) Effects of ice coverage and ice-rafted material on sedimentation
392 in the Fram Strait. *Nature* 350: 409–411. DOI: <https://doi.org/10.1038/350409a0>.

393 Hebbeln D, Dokken TM, Andersen ES, et al. (1994) Moisture supply for northern ice-sheet
394 growth during the Last Glacial Maximum. *Nature* 370: 357–360.

395 Hopkins TS (1991) The GIN Sea-A synthesis of its physical oceanography and literature review
396 1972-1985. *Earth Science Reviews* 30(3–4): 175–318. DOI: 10.1016/0012-
397 8252(91)90001-V.

398 Jang K, Bayon G, Vogt C, et al. (2023) Non-linear response of glacier melting to Holocene
399 warming in Svalbard recorded by sedimentary iron (oxyhydr)oxides. *Earth and Planetary*
400 *Science Letters* 607. Elsevier B.V.: 118054. DOI: 10.1016/j.epsl.2023.118054.

401 Johnsen SJ, Dahl-Jensen D, Gundestrup NS, et al. (2001) Oxygen isotope and
402 palaeotemperature records from six Greenland ice-core stations: Camp Century, Dye-3,
403 GRIP, GISP2, Renland and NorthGRIP. *Journal of Quaternary Science* 16(4): 299–307.
404 DOI: 10.1002/jqs.622.

405 Klitgaard-Kristensen D, Rasmussen TL and Koç N (2013) Palaeoceanographic changes in the
406 northern Barents Sea during the last 16000 years - new constraints on the last deglaciation
407 of the Svalbard-Barents Sea Ice Sheet. *Boreas* 42(3): 798–813. DOI: 10.1111/j.1502-
408 3885.2012.00307.x.

- 409 Knies J, Pathirana I, Cabedo-Sanz P, et al. (2017) Sea-ice dynamics in an Arctic coastal polynya
410 during the past 6500 years. *Arktos* 3(1). Springer International Publishing: 1. DOI:
411 10.1007/s41063-016-0027-y.
- 412 Kujawa A, Łacka M, Szymańska N, et al. (2021) Could Norwegian fjords serve as an analogue
413 for the future of the Svalbard fjords? State and fate of high latitude fjords in the face of
414 progressive “atlantification”. *Polar Biology* 44(12): 2217–2233. DOI: 10.1007/s00300-
415 021-02951-z.
- 416 Kunz-Pirrung M (1998) Rekonstruktion der Oberflächenwassermassen der östlichen Laptevsee
417 im Holozän anhand von aquatischen Palynomorphen. *Berichte zur Polarforschung* 281:
418 1–117.
- 419 Łacka M, Zajączkowski M, Forwick M, et al. (2015) Late Weichselian and Holocene
420 paleoceanography of Storfjordrenna, southern Svalbard. *Climate of the Past* 11: 587–603.
421 DOI: 10.5194/cpd-10-3053-2014.
- 422 Łacka M, Cao M, Rosell-Melé A, et al. (2019) Postglacial paleoceanography of the western
423 Barents Sea: Implications for alkenone-based sea surface temperatures and primary
424 productivity. *Quaternary Science Reviews* 224. DOI: 10.1016/j.quascirev.2019.105973.
- 425 Łacka M, Michalska D, Pawłowska J, et al. (2020) Multiproxy paleoceanographic study from
426 the western Barents Sea reveals dramatic Younger Dryas onset followed by oscillatory
427 warming trend. *Scientific Reports* 10(1): 15667. DOI: 10.1038/s41598-020-72747-4.
- 428 Laskar J, Robutel P, Joutel F, et al. (2004) A long-term numerical solution for the insolation
429 quantities of the Earth. *Astronomy & Astrophysics* 428(1): 261–285. DOI: 10.1051/0004-
430 6361:20041335.
- 431 Lien VS, Schlichtholz P, Skagseth Ø, et al. (2017) Wind-Driven Atlantic Water Flow as a Direct
432 Mode for Reduced Barents Sea Ice Cover. *Journal of Climate* 30(2): 803–812. DOI:
433 10.1175/jcli-d-16-0025.1.
- 434 Loeng H (1991) Features of the physical oceanographic conditions of the Barents Sea. *Polar*
435 *Research* 10(1): 5–18. DOI: 10.1111/j.1751-8369.1991.tb00630.x.
- 436 Mangerud J, Bondevik S, Gulliksen S, et al. (2006) Marine 14C reservoir ages for 19th century
437 whales and molluscs from the North Atlantic. *Quaternary Science Reviews* 25(23–24):
438 3228–3245. DOI: 10.1016/j.quascirev.2006.03.010.

- 439 Manley TO (1995) Branching of Atlantic Water within the Greenland-Spitsbergen Passage: An
440 estimate of recirculation. *Journal of Geophysical Research* 100(C10): 20,627-20,634.
441 DOI: 10.1029/95JC01251.
- 442 Matul A, Spielhagen RF, Kazarina G, et al. (2018) Warm-water events in the eastern Fram
443 Strait during the last 2000 years as revealed by different microfossil groups. *Polar*
444 *Research* 37(1). Routledge. DOI: 10.1080/17518369.2018.1540243.
- 445 McDermott F, Matthey DP and Hawkesworth C (2001) Centennial-scale Holocene climate
446 variability revealed by a high-resolution speleothem $\delta^{18}\text{O}$ record from SW Ireland.
447 *Science* 294(1328–1331). DOI: 10.1126/science.1063678.
- 448 McKay NP, Kaufman DS, Routsos CC, et al. (2018) The Onset and Rate of Holocene
449 Neoglacial Cooling in the Arctic. *Geophysical Research Letters* 45(22): 12,487-12,496.
450 DOI: 10.1029/2018GL079773.
- 451 Mertens KN, Verhoeven K, Verleye T, et al. (2009) Determining the absolute abundance of
452 dinoflagellate cysts in recent marine sediments: The *Lycopodium* marker-grain method put
453 to the test. *Review of Palaeobotany and Palynology* 157(3–4): 238–252. DOI:
454 10.1016/j.revpalbo.2009.05.004.
- 455 Mertens KN, Rengefors K, Moestrup Ø, et al. (2012) A review of recent freshwater
456 dinoflagellate cysts: Taxonomy, phylogeny, ecology and palaeocology. *Phycologia* 51(6):
457 612–619. DOI: 10.2216/11-89.1.
- 458 Mertens KN, Price AM and Pospelova V (2012) Determining the absolute abundance of
459 dinoflagellate cysts in recent marine sediments II: Further tests of the *Lycopodium* marker-
460 grain method. *Review of Palaeobotany and Palynology* 184. Elsevier B.V.: 74–81. DOI:
461 10.1016/j.revpalbo.2012.06.012.
- 462 Mertens KN, Yamaguchi A, Takano Y, et al. (2013) A New Heterotrophic Dinoflagellate from
463 the North-eastern Pacific, *Protoperidinium fukuyoi*: Cyst-Theca Relationship, Phylogeny,
464 Distribution and Ecology. *Journal of Eukaryotic Microbiology* 60(6): 545–563. DOI:
465 10.1111/jeu.12058.
- 466 Mertens KN, Takano Y, Gu H, et al. (2015) Cyst-theca relationship of a new dinoflagellate with
467 a spiny round brown cyst, *Protoperidinium lewisiae* sp. nov., and its comparison to the
468 cyst of *Oblea acanthocysta*. *Phycological Research* 63(2): 110–124. DOI:
469 10.1111/pre.12083.

- 470 Moestrup Ø, Lindberg K and Daugbjerg N (2009) Studies on woloszynskioid dinoflagellates
471 IV: The genus *Biecheleria* gen. nov. *Phycological Research* 57(3): 203–220. DOI:
472 10.1111/j.1440-1835.2009.00540.x.
- 473 Montresor M, Procaccini G and Stoecker DK (1999) *Polarella glacialis*, gen. nov., sp. nov.
474 (Dinophyceae): Suessiaceae are still alive! *Journal of Phycology* 35: 186–197.
- 475 Müller J, Wagner A, Fahl K, et al. (2011) Towards quantitative sea ice reconstructions in the
476 northern North Atlantic: A combined biomarker and numerical modelling approach. *Earth
477 and Planetary Science Letters* 306(3–4). Elsevier B.V.: 137–148. DOI:
478 10.1016/j.epsl.2011.04.011.
- 479 Müller J, Werner K, Stein R, et al. (2012) Holocene cooling culminates in sea ice oscillations
480 in Fram Strait. *Quaternary Science Reviews* 47. Elsevier Ltd: 1–14. DOI:
481 10.1016/j.quascirev.2012.04.024.
- 482 Olsen J, Anderson NJ and Knudsen MF (2012) Variability of the North Atlantic Oscillation
483 over the past 5,200 years. *Nature Geoscience* 5(11). Nature Publishing Group: 808–812.
484 DOI: 10.1038/ngeo1589.
- 485 Orme LC, Miettinen A, Divine D V., et al. (2018) Subpolar North Atlantic sea surface
486 temperature since 6 ka BP: Indications of anomalous ocean-atmosphere interactions at 4-
487 2 ka BP. *Quaternary Science Reviews* 194. Elsevier Ltd: 128–142. DOI:
488 10.1016/J.QUASCIREV.2018.07.007.
- 489 Overland JE and Wang M (2013) When will the summer Arctic be nearly sea ice free?
490 *Geophysical Research Letters* 40(10): 2097–2101. DOI: 10.1002/grl.50316.
- 491 Paasche Ø and Bakke J (2009) The Holocene Turnover - A global climatic shift at ~4 Ka.
492 *Geophysical Research Abstracts* 11. Vienna: Copernicus: EGU2009-14017. Available at:
493 <https://meetings.copernicus.org/egu2009/>.
- 494 Paasche Ø, Løvlie R, Dahl SO, et al. (2004) Bacterial magnetite in lake sediments: Late glacial
495 to Holocene climate and sedimentary changes in northern Norway. *Earth and Planetary
496 Science Letters* 223(3–4): 319–333. DOI: 10.1016/j.epsl.2004.05.001.
- 497 Pawłowska J, Łacka M, Kucharska M, et al. (2020) Multiproxy evidence of the Neoglacial
498 expansion of Atlantic Water to eastern Svalbard. *Climate of the Past* 16(2): 487–501. DOI:
499 10.5194/cp-16-487-2020.

- 500 Pfirman SL, Bauch D and Gammelsrød T (1994) The Northern Barents Sea: Water Mass
501 Distribution and Modification. In: Johannessen OM, Muench RD, and Overland JE (eds)
502 *The Polar Oceans and Their Role in Shaping the Global Environment, Volume 85.*
503 *Geophysica*. American Geophysical Union, pp. 77–94.
- 504 Pospelova V and Head MJ (2002) *Islandinium brevispinosum* sp. nov. (Dinoflagellata), a new
505 organic-walled dinoflagellate cyst from modern estuarine sediments of New England
506 (USA). *Journal of Phycology* 38(3): 593–601. DOI: 10.1046/j.1529-8817.2002.01206.x.
- 507 Pospelova V, Chmura GL, Boothman WS, et al. (2005) Spatial distribution of modern
508 dinoflagellate cysts in polluted estuarine sediments from Buzzards Bay (Massachusetts,
509 USA) embayments. *Marine Ecology Progress Series* 292(Taylor 1987): 23–40. DOI:
510 10.3354/meps292023.
- 511 Pospelova V, Esenkulova S, Johannessen SC, et al. (2010) Organic-walled dinoflagellate cyst
512 production, composition and flux from 1996 to 1998 in the central Strait of Georgia (BC,
513 Canada): A sediment trap study. *Marine Micropaleontology* 75(1–4). Elsevier B.V.: 17–
514 37. DOI: 10.1016/j.marmicro.2010.02.003.
- 515 Prange M and Lohmann G (2003) Effects of mid-Holocene river runoff on the Arctic ocean/sea-
516 ice system: a numerical model study. *The Holocene* 13(3): 335–342. DOI:
517 10.1191/0959683603hl626rp.
- 518 Ramseier RO, Garrity C, Bauerfeind E, et al. (1999) Sea-ice impact on long-term particle flux
519 in the Greenland Sea's Is Odden-Nordbukta region, 1985-1996. *Journal of Geophysical*
520 *Research* 104(C3): 5329–5343. DOI: 10.1029/1998jc900048.
- 521 Reimer PJ and Reimer RW (2001) A marine reservoir correction database and on-line interface.
522 *Radiocarbon* 43(2 PART I): 461–463. DOI: 10.1017/s0033822200038339.
- 523 Renssen H (2022) Climate model experiments on the 4.2 ka event: The impact of tropical sea-
524 surface temperature anomalies and desertification. *Holocene* 32(5): 378–389. DOI:
525 10.1177/09596836221074031.
- 526 Rigual-Hernández AS, Colmenero-Hidalgo E, Martrat B, et al. (2017) Svalbard ice-sheet decay
527 after the Last Glacial Maximum: new insights from micropalaeontological and organic
528 biomarker paleoceanographical reconstructions. *Palaeogeography, Palaeoclimatology,*
529 *Palaeoecology* 465. Elsevier B.V.: 225–236. DOI: 10.1017/CBO9781107415324.004.

- 530 Risebrobakken B, Moros M, Ivanova E V., et al. (2010) Climate and oceanographic variability
531 in the SW Barents Sea during the Holocene. *The Holocene* 20(4): 609–621. DOI:
532 10.1177/0959683609356586.
- 533 Rochon A, de Vernal A, Turon J-L, et al. (1999) Distribution of recent dinoflagellate cysts in
534 surface sediments from the North Atlantic Ocean and adjacent seas in relation to sea-
535 surface parameters. *American Association of Stratigraphic Palynologists Contribution*
536 *Series* 35: 1–146. Available at: <https://epic.awi.de/id/eprint/3706/>.
- 537 Rudels B, Korhonen M, Schauer U, et al. (2015) Circulation and transformation of Atlantic
538 water in the Eurasian Basin and the contribution of the Fram Strait inflow branch to the
539 Arctic Ocean heat budget. *Progress in Oceanography* 132. Elsevier Ltd: 128–152. DOI:
540 10.1016/j.pocean.2014.04.003.
- 541 Sakshaug E (2004) Primary and Secondary Production in the Arctic Seas. In: Stein R and
542 Macdonald RW (eds) *The Organic Carbon Cycle in the Arctic Ocean*. Berlin Heidelberg:
543 Springer, pp. 57–81. DOI: https://doi.org/10.1007/978-3-642-18912-8_3.
- 544 Sarnthein M, van Kreveland S, Erlenkeuser H, et al. (2003) Centennial-to-millennial-scale
545 periodicities of Holocene climate and sediment injections off the western Barents shelf,
546 75°N. *Boreas* 32: 447–461. DOI: 10.1080/03009480310003351.
- 547 Schauer U, Loeng H, Rudels B, et al. (2002) Atlantic Water flow through the Barents and Kara
548 Seas. *Deep-Sea Research Part I: Oceanographic Research Papers* 49(12): 2281–2298.
549 DOI: 10.1016/S0967-0637(02)00125-5.
- 550 Serreze MC and Francis JA (2006) The Arctic amplification debate. *Climatic Change* 76(3–4):
551 241–264. DOI: 10.1007/s10584-005-9017-y.
- 552 Smik L, Cabedo-Sanz P and Belt ST (2016) Semi-quantitative estimates of paleo Arctic sea ice
553 concentration based on source-specific highly branched isoprenoid alkenes: A further
554 development of the PIP25 index. *Organic Geochemistry* 92. Elsevier Ltd: 63–69. DOI:
555 10.1016/j.orggeochem.2015.12.007.
- 556 Sorteberg A and Kvingedal B (2006) Atmospheric forcing on the Barents Sea winter ice extent.
557 *Journal of Climate* 19(19): 4772–4784. DOI: 10.1175/JCLI3885.1.
- 558 Spielhagen RF, Werner K, Aagaard-Sørensen S, et al. (2011) Enhanced Modern Heat Transfer
559 to the Arctic by Warm Atlantic Water. *Science* 331: 450–453. DOI:

560 10.1126/science.1197397.

561 Stuiver M and Reimer PJ (1993) Radiocarbon calibration program. *Radiocarbon* 35: 215–230.

562 Svendsen JI and Mangerud J (1997) Holocene glacial and climatic variations on Spitsbergen,
563 Svalbard. *The Holocene* 7(1): 45–57.

564 Telesiński MM, Spielhagen RF and Bauch HA (2014) Water mass evolution of the Greenland
565 Sea since late glacial times. *Climate of the Past* 10: 123–136. DOI: 10.5194/cp-10-123-
566 2014.

567 Telesiński MM, Bauch HA, Spielhagen RF, et al. (2015) Evolution of the central Nordic Seas
568 over the last 20 thousand years. *Quaternary Science Reviews* 121: 98–109. DOI:
569 10.1016/j.quascirev.2015.05.013.

570 Telesiński MM, Pospelova V, Mertens KN, et al. (2023) Dinoflagellate cysts and benthic
571 foraminifera from surface sediments of Svalbard fjords and shelves as paleoenvironmental
572 indicators. *Oceanologia* 65(4): 571–594. DOI: 10.1016/j.oceano.2023.06.007.

573 Tesi T, Muschitiello F, Mollenhauer G, et al. (2021) Rapid Atlantification along the Fram Strait
574 at the beginning of the 20th century. *Science Advances* 7(48). DOI:
575 10.1126/sciadv.abj2946.

576 Thackeray CW and Hall A (2019) An emergent constraint on future Arctic sea-ice albedo
577 feedback. *Nature Climate Change* 9(12). Springer US: 972–978. DOI: 10.1038/s41558-
578 019-0619-1.

579 Thomson J, Croudace IW and Rothwell RG (2006) A geochemical application of the ITRAX
580 scanner to a sediment core containing eastern Mediterranean sapropel units. *Geological*
581 *Society Special Publication* 267: 65–77. DOI: 10.1144/GSL.SP.2006.267.01.05.

582 Vinje T (1977) Sea ice conditions in the European sector of the marginal seas of the Arctic,
583 1966-1975. *Norsk Polarinstitut Årbok*: 163–174.

584 Vinje T (2001) Anomalies and trends of sea-ice extent and atmospheric circulation in the Nordic
585 Seas during the period 1864-1998. *Journal of Climate* 14(3): 255–267. DOI:
586 10.1175/1520-0442(2001)014<0255:AATOSI>2.0.CO;2.

587 Walczowski W and Piechura J (2007) Pathways of the Greenland Sea warming. *Geophysical*
588 *Research Letters* 34(10): 5. DOI: 10.1029/2007GL029974.

- 589 Walczowski W and Piechura J (2011) Influence of the West Spitsbergen Current on the local
590 climate. *International Journal of Climatology* 31(7): 1088–1093. DOI: 10.1002/joc.2338.
- 591 Walker MJC, Head MJ, Lowe J, et al. (2019) Subdividing the Holocene Series/Epoch:
592 formalization of stages/ages and subseries/subepochs, and designation of GSSPs and
593 auxiliary stratotypes. *Journal of Quaternary Science* 34(3). John Wiley & Sons, Ltd: 173–
594 186. DOI: 10.1002/jqs.3097.
- 595 Wang T, Surge D and Mithen S (2012) Seasonal temperature variability of the Neoglacial
596 (3300-2500BP) and Roman Warm Period (2500-1600BP) reconstructed from oxygen
597 isotope ratios of limpet shells (*Patella vulgata*), Northwest Scotland. *Palaeogeography,*
598 *Palaeoclimatology, Palaeoecology* 317–318. Elsevier B.V.: 104–113. DOI:
599 10.1016/j.palaeo.2011.12.016.
- 600 Wanner H (2021) Late-Holocene: Cooler or warmer? *The Holocene* 31(9): 1501–1506. DOI:
601 10.1177/09596836211019106.
- 602 Wassmann P (2011) Arctic marine ecosystems in an era of rapid climate change. *Progress in*
603 *Oceanography* 90(1–4): 1–17. DOI: 10.1016/j.pocean.2011.02.002.
- 604 Wassmann P, Reigstad M, Haug T, et al. (2006) Food webs and carbon flux in the Barents Sea.
605 *Progress in Oceanography* 71(2–4): 232–287. DOI: 10.1016/j.pocean.2006.10.003.
- 606 Werner K, Spielhagen RF, Bauch D, et al. (2013) Atlantic Water advection versus sea-ice
607 advances in the eastern Fram Strait during the last 9 ka: Multiproxy evidence for a two-
608 phase Holocene. *Paleoceanography* 28: 283–295. DOI: 10.1002/palo.20028.
- 609 Zonneveld KAF (1997) New species of organic walled dinoflagellate cysts from modern
610 sediments of the Arabian Sea (Indian Ocean). *Review of Palaeobotany and Palynology*
611 97(3–4): 319–337. DOI: 10.1016/S0034-6667(97)00002-X.
- 612 Zonneveld KAF and Pospelova V (2015) A determination key for modern dinoflagellate cysts.
613 *Palynology* 39(3): 387–409. DOI: 10.1080/01916122.2014.990115.

614 **Figure captions**

615 Fig. 1. Schematic map showing present-day surface water circulation in the Barents Sea.
616 Red arrows indicate Atlantic Water, light blue arrows – Polar/Arctic Water, white dashed line
617 – Arctic Front (AF). The location of core JM09-020 is marked with an asterisk. The location of
618 core NP05-11-70GC (Berben et al., 2017) also discussed in the paper is marked with a dot. BIC

619 – Bear Island Current, ESC – East Spitsbergen Current, NCaC – North Cape Current, NwAC –
620 Norwegian Atlantic Current, WSC – West Spitsbergen Current.

621 Fig. 2. Dinocyst record of core JM09-020. a) Total dinocyst abundance [cysts g⁻¹]. b)
622 Relative abundance of autotrophic vs. heterotrophic species. c) Absolute [cysts g⁻¹] and relative
623 [%] abundance of *Echinidinium karaense*. d) Absolute [cysts g⁻¹] and relative [%] abundance
624 of *Operculoidinium centrocarpum* s.l.

625 Fig. 3. Paleoceanographic proxies of Late Holocene changes in the northwestern Barents
626 Sea from cores JM09-020 (a-f) and NP05-11-70GC (g). a) Absolute dinocyst abundance [cysts
627 g⁻¹]. b) Absolute [cysts g⁻¹] and relative [%] abundance of *Echinidinium karaense*. c) Relative
628 [%] abundance of *Operculoidinium centrocarpum* s.l. and *Islandinium minutum*. d) Alkenone-
629 based sea-surface temperature reconstruction (Łącka et al., 2019). Thin line – raw data, thick
630 line – 3 pt moving average. e) Stable carbon isotope ratios [‰ vs VPDB] of benthic foraminifera
631 *Elphidium clavatum* (Łącka et al., 2015). f) Ba/Ti elemental ratios as obtained from XRF core
632 scanning (Łącka et al., 2015). Thin line – raw data, thick line – 5 pt moving average. G) P_{III}IP₂₅
633 index and spring sea-ice concentration (SpSIC) [%] calculated from it (Berben et al., 2017).
634 The horizontal dashed line marks the 0.8 P_{III}IP₂₅ threshold, indicating >5% summer sea-ice
635 concentration.

Fig. 1

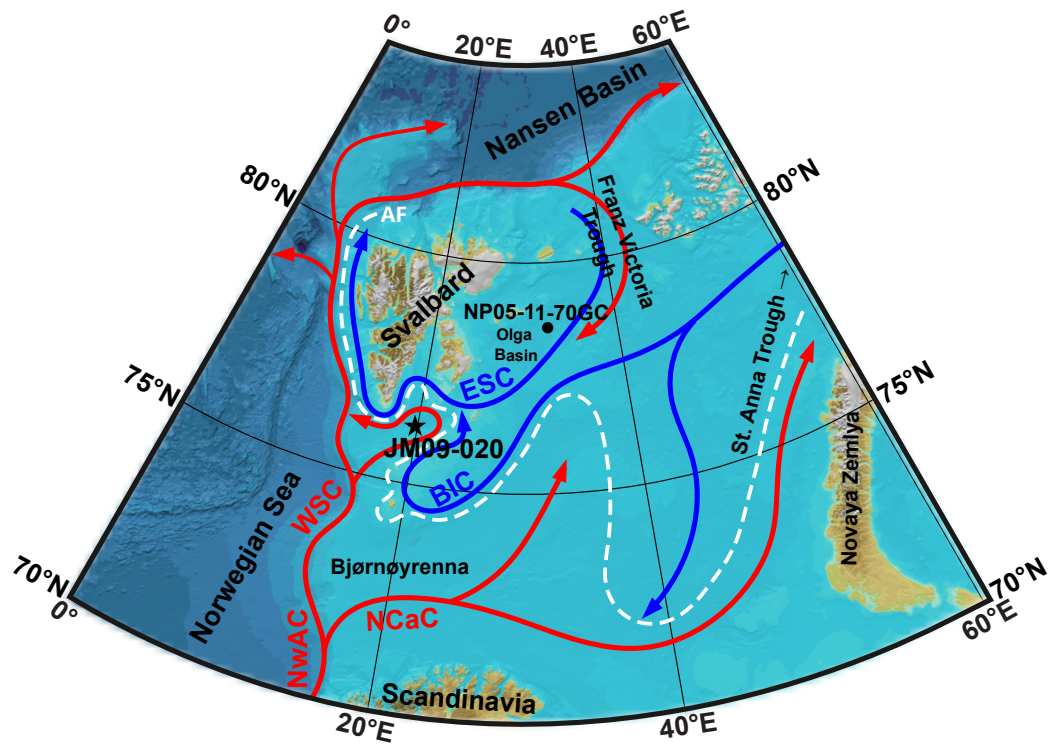


Fig. 2

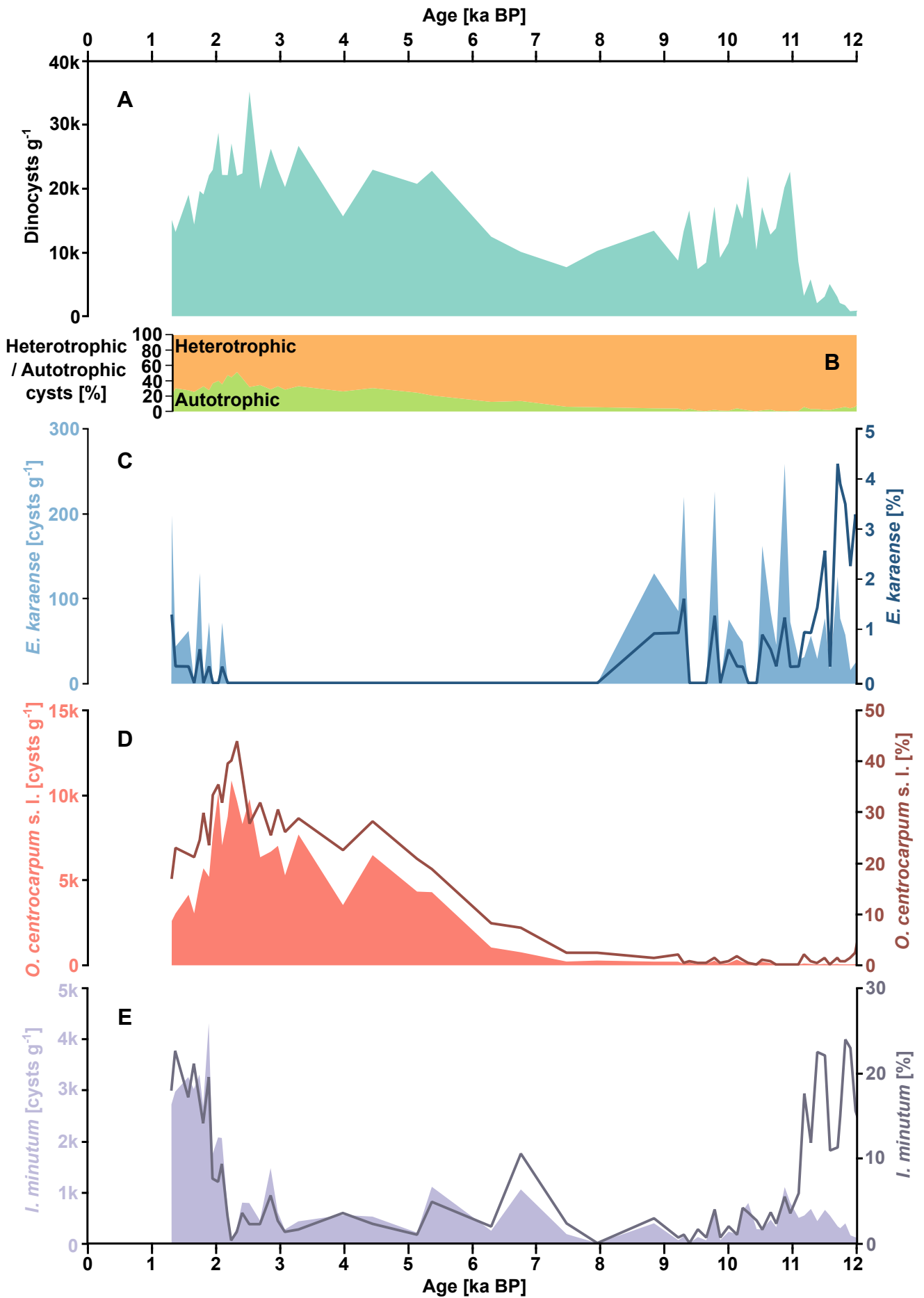


Fig. 3

